Advances in Engineering Research : Possibilities and Challenges
ISSN Print: 3079-5192
ISSN Online: 3079-5206
https://doi.org/10.63313/AERpc.9011

Detection method of tubing coupling based on magnetic field induction

Meng Yang*. Mingjiang Shi
School of Mechanical Engineering, Southwest Petroleum University, Chengdu, China
Email: swpu_wzj@163.com

How to cite this paper: Yang, M., & Shi, M. J. (2025). Detection method of tubing coupling based on magnetic field induction. Advances in Engineering Research: Possibilities and Challenges, 1(2), 23–33. ISSN Print:3079-5192; ISSN Online: 3079-5206. https://doi.org/10.63313/AERpc.9011
Published: 2025-04-29

Abstract

The inspection of tubing coupling is a key part to ensure the safety of snub-bing operation, To realize the accurate identification of tubing and coupling, Studied a magnetic detection method, Accurate identification of coupling by capturing the difference in magnetic field strength between the surface of the oil pipe and the coupling, This paper uses COMSOL software to establish a finite element simulation model of the pipe coupling detection device. Through simu-lation calculations, the effects of the spacing between magnetic materials, per-manent magnet strength, pipe eccentricity, and coupling defects on the detec-tion performance are studied. The influence patterns of different factors on the detection results are obtained, and finally, experiments are conducted to verify the feasibility of the method.

Keywords

Snubbing Operation; Coupling Detection; Magnetic Testing Method; Finite Ele-Ment Analysis

1. Introduction

Since the emergence of pressurized operations in the 1920s, it has gradually become a new trend in workover operations. Since 2010, China has been promoting this technology on a large scale, and a pressurized operation technology suitable for different well conditions has been initially formed. (Qun LEI et al., 2019&2020) During the process of lowering the tubing in pressurized operations, the collar diameter is larger than the tubing diameter, and forcing it through the blowout preventer (BOP) can cause wear to the rubber core, reducing its service life and increasing the risk of pressurized operations. Therefore, accurately detecting the collar position and controlling the opening and closing of the blowout preventer to allow the collar to safely pass through the wellhead is crucial for achieving automated pressurized operations.

Currently, the main methods for detecting tubing collars include contact-based collar detection, electromagnetic collar detection, and image-based collar detection. (Ni, XH ,et al.,2014& Wang, YK ,et al.,2019)Contact-based collar detection detects the collar by measuring displacement changes when the collar comes into contact with the detection roller. However, this method is susceptible to errors caused by downhole metal or non-metallic impurities, and the detection roller can cause wear on the collar. Electromagnetic collar detection identifies the collar by detecting changes in the magnetic field at the collar's position, but the high temperature and pressure conditions at the wellhead require temperature compensation and other adjustments for the probe. Image-based collar detection uses digital image processing and image recognition technology to detect tubing collars via video. The effectiveness of this method not only requires the recognition algorithm to be highly accurate but also faces challenges due to the lightless environment caused by pressure-sealing, which makes it difficult to meet the conditions for image detection.

This paper is based on the principle of magnetic detection, using permanent magnets to generate a constant magnetic field combined with the Hall effect to achieve accurate identification of tubing collars. Finite element simulation was conducted, and a finite element simulation model of the tubing collar detection device was established using COMSOL software. Through simulation calculations, the effects of various factors on the detection performance were studied, including the distance between magnetic conductors, the strength of the permanent magnets, tubing eccentricity, and collar defects. The influence patterns of these factors on the detection performance were obtained. A detection device for pipe coupling defects was designed, and an experimental platform was built for experimental analysis.

2. Theoretical basis of magnetic Flux Testing

The magnetic flux detection method detects rod-shaped wear defects and large-area corrosion defects by measuring the changes in magnetic flux in the tubing magnetic circuit using magnetic-sensitive sensors arranged in a magnetizing loop.(Dost, Y.,Apaydın,et al,2012) According to Kirchhoff's First Law (the principle of magnetic flux continuity), the algebraic sum of the magnetic flux at any node (on a closed surface) in the magnetic circuit is zero, indicating that magnetic flux is conserved in the magnetic circuit. Magnetic flux is the surface integral of the magnetic field intensity, and it is typically represented by the number of magnetic flux lines passing through a surface.

The differential form of Maxwell's equations is mathematically expressed as follows:

$$d\phi = B_n dS = B\cos\theta dS = B \cdot dS \qquad (1\text{-}1)$$

$$\phi = BS \qquad (1\text{-}2)$$

In the equation, $\boldsymbol{B_n}$ represents the component of the magnetic flux density B that is perpendicular to the surface element S. $\boldsymbol{\theta}$ is the angle between the normal direction of the surface element and the magnetic flux density.

Magnetic flux detection can be simplified using the equivalent magnetic circuit method. During detection, the propagation path of the magnetic flux lines can be simplified as shown in Fig.1. Since the magnetic permeability of the magnetic yoke is much greater than that of air, the amount of magnetic flux leaking from the yoke into the air is very small and can be neglected. The magnetic circuit in Fig.1 is equivalent to the circuit diagram in the figure. From the Ohm's law of the magnetic circuit, the following can be obtained.

$$R_{a1}\phi_1 + R_y\phi_2 + R_c\phi_3 = F \tag{1-3}$$

$$\phi_1 = \phi_2 + \phi_4 \tag{1-4}$$

$$\phi_2 = \phi_3 + \phi_5 \tag{1-5}$$

$$R_c\phi_3 = R_{a3}\phi_5 \tag{1-6}$$

$$R_y\phi_2 + R_c\phi_3 = R_{a2}\phi_4 \tag{1-7}$$

In the equation, $\boldsymbol{F}$ is the magnetomotive force of the permanent magnet, $\boldsymbol{R_{a1}}$is the magnetic reluctance of the air gap between the magnet and the measured oil pipe, $\boldsymbol{R_{a2}}$ is the equivalent magnetic reluctance of magnetic circuits ②, ③, and ④, and $\boldsymbol{R_{a3}}$ is the air reluctance parallel to the measured oil pipe in magnetic circuit ⑤. $\boldsymbol{R_y}$ is the magnetic reluctance of the magnetic yoke, $\boldsymbol{R_c}$ is the magnetic reluctance of the measured oil pipe, and $\emptyset_1$, $\emptyset_2$, $\emptyset_3$, $\emptyset_4$, and $\emptyset_5$ represent the magnetic flux passing through the permanent magnet, the magnetic yoke, the measured oil pipe, $\boldsymbol{R_{a2}}$, and $\boldsymbol{R_{a3}}$, respectively. The solution can be obtained by solving the above equation simultaneously.

$$\phi_5 = \frac{R_c(\phi_1 - \phi_4)}{R_{a3} + R_c} \tag{1-8}$$

For specimens made of ferromagnetic materials such as steel or similar alloys, their relative permeability is greater than that of air. Due to the magnetic reluctance, the magnetic flux density through the specimen will be higher than that in the air. From equation (1-8), it can be seen that when the coupling arrives, $\boldsymbol{R_c}$ increases, $\boldsymbol{R_{a3}}$ decreases, and the changes in $\emptyset_1$ and $\emptyset_4$ can be ignored, which leads to the increase of $\emptyset_5$. Therefore, the magnetic flux density at the surface of the specimen (air gap) will be smaller than before. The detection of whether the coupling has arrived is thus transformed into capturing the change in magnetic flux density.

3. Finite element simulation model

The geometric model in this paper is constructed by directly drawing geometric objects.(Shi, MJ,et al.,2018& Jomdecha, C.,Prateepasen,et al.,2009) To make the final simulation results more similar to the actual situation, a three-dimensional model is chosen. With the excitation source being a permanent magnet. The flux variation of the coupling in the static magnetic field is analyzed. A three-dimensional model for coupling detection is established by simulating the actual shapes of the oil pipe and the coupling, as shown in Fig.1 (the air domain and infinite element domain have been hidden). The model consists of the oil pipe, coupling, air domain, permanent magnet, magnetic conductor, and other components.

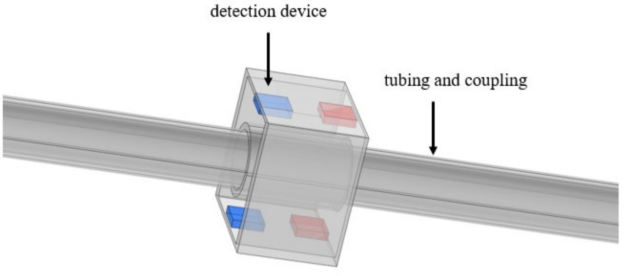

Fig.1 Three-dimensional simulation model without defects

The geometric parameters of each part of the model are shown in Table 1.

Table 1. The key parameters of the simulation model

model parameter	Model length (mm)	Model thickness (mm)
tubing	1000	5.5
coupling	130	8.5
permanent magnet	50	15
magnetic conductor	120	10
air domain	2000	1000

A parametric scan is added in the model study to simulate the process of the oil pipe entering and exiting the detection device during the inspection. The variation of the magnetic flux density in the three axial directions at the detection point is solved and shown in Fig2. The magnetic flux density in the figure is displayed with both positive and negative values, indicating the direction of the magnetic flux density.

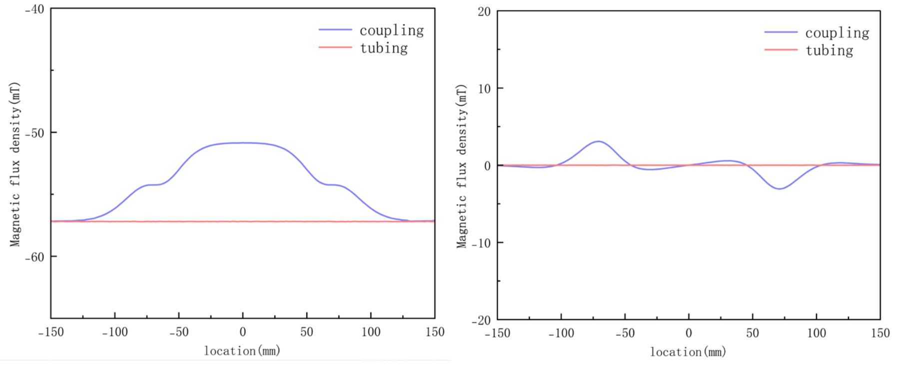

(a) Axial components (b) Radial component

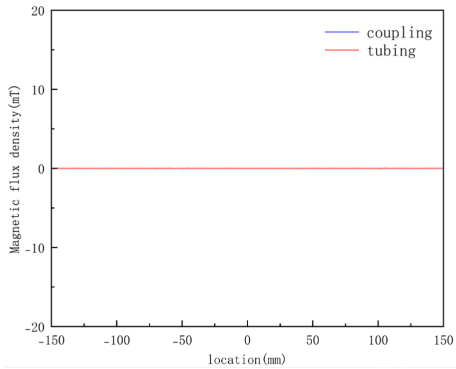

(c) Circumferential components

Fig.2 Magnetic flux density components of the pipe coupling detection magnetic signal

To investigate the best detection effect for the oil pipe coupling, this section simulates various factors that influence the detection effect to obtain the optimal performance of the detection device. Through the analysis of the model's magnetic circuit, the factors that mainly affect the detection of the oil pipe coupling are: the structure of the detection device, the detection position, the eccentricity of the oil pipe, and defects in the oil pipe. The following will separately study the influence of each factor on the axial magnetic flux density when the coupling and oil pipe pass through the detection device.

3.1. The influence of the magnetic conductor spacing on the variation of magnetic flux den-sity

Set the magnetic conductor spacing as the only variable, with values of 100mm, 120mm, 140mm, 160mm, and 180mm. Simulate the detection device under two conditions: with and without a coupling passing through (oil pipe). A parametric scan is performed to obtain the variation of axial and radial magnetic flux density at the detection point with the magnetic conductor spacing, as shown in Fig.3.

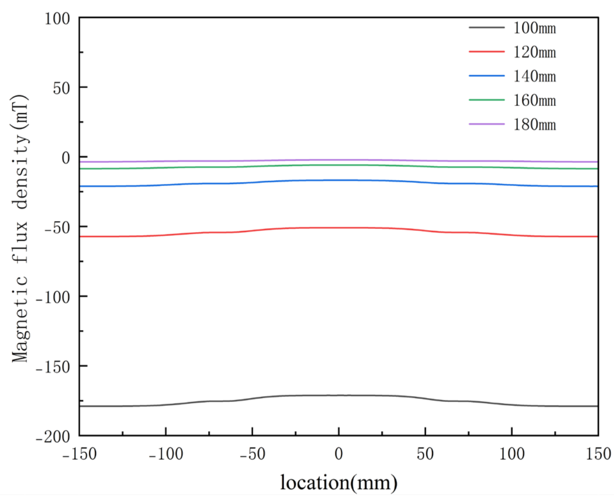

Fig.3 Axial magnetic flux density at different magnetic material spacings

Since the axial magnetic flux density variation of the coupling and oil pipe cannot be visually observed directly from the figure, the axial magnetic flux density values corresponding to the coupling and the oil pipe at the detection center are extracted, as shown in Table 2.

Table 2. The effect of the spacing between magnetic materials on the axial magnetic flux variation

Spacing (mm)	100	120	140	160	180
No coupling flux(mT)	178.81	57.16	21.19	8.57	3.67
coupling flux(mT)	171.09	50.85	16.82	5.92	2.17
flux change	7.72	6.31	4.37	2.65	1.50

Result analysis: Under the influence of the magnetic conductor spacing as a single variable factor, the variation of magnetic flux density is maximum when the spacing is 100mm. As the magnetic conductor spacing continues to increase, the variation of magnetic flux density gradually decreases. In summary, the selection of magnetic conductor spacing should be as small as possible.

3.2. The influence of magnetization intensity on the variation of magnetic flux density.

Set the magnetization intensity as the only variable, with values of 1.0T, 1.1T, 1.2T, 1.3T, and 1.4T. The axial magnetic flux density variations of the coupling and oil pipe are studied and calculated, as shown in Table 3.

Table 3. The effect of magnetic field strength on the axial magnetic flux variation

Residual magnetic flux mode(T)	1.0	1.1	1.2	1.3	1.4
No coupling flux(mT)	35.72	43.49	51.25	59.02	66.78
coupling flux(mT)	32.86	40.00	47.15	54.29	61.44
flux change	2.86	3.49	4.10	4.73	5.34

From the data in the table, it can be observed that as the magnetic field strength increases, the axial magnetic flux density also increases. At the same time, the magnetic flux variation in the coupling and oil pipe also increases, showing an approximately linear relationship. To achieve the best detection results, the magnetization intensity should be chosen to be as strong as possible within the sensor's measurement range.

3.3. The influence of oil pipe eccentricity on the variation of magnetic flux density

To study the effect of eccentricity on detection, the eccentric angle is fixed at 0 degrees, meaning the eccentricity occurs along the axial direction. The eccentric distances are set to 3, 6, 9, 12, and 15 mm, and the magnetic flux density variation at the detection points under various conditions is simulated, as shown in Table 4.

Table 4. The effect of pipe eccentricity on the axial magnetic flux variation

Eccentricity(mm)	3	6	9	12	15
No coupling flux(mT)	55.61	53.49	50.56	46.51	40.97
coupling flux(mT)	46.96	41.62	34.44	25.24	14.65
flux change	8.65	11.87	16.12	21.27	26.32

Result analysis: From the data in the table, it can be seen that as the eccentricity increases, both the magnetic flux density without the coupling and with the coupling decrease. Comparing with Table 3-2, it can be observed that when the eccentricity is around 9 mm, the magnetic flux density without the coupling is approximately equal to the magnetic flux density with the coupling when there is no eccentricity. This situation can easily lead to misdetection.

To study the effect of eccentric angle on detection, the eccentric distance is fixed at 3 mm, and the eccentric angles are set to 15°, 30°, 45°, 60°, 75°, and 90°. The magnetic flux density variation at the detection points under various conditions is simulated, as shown in Table 5.

Table 5. The effect of pipe eccentricity on the axial magnetic flux variation

Eccentric Angle (mm)	15°	30°	45°	60°	75°
No coupling flux(mT)	55.68	55.86	56.14	56.47	56.83
coupling flux(mT)	47.11	47.58	48.28	49.12	50.03
flux change	10.57	8.28	7.86	7.35	6.8

Result analysis: From the data in the table, it can be observed that as the eccentric angle increases, both the magnetic flux density without the coupling and with the coupling increase. Comparing with Table 3-2, it can be found that when the eccentric angle is 90°, the magnetic flux density with the coupling is approximately equal to the magnetic flux density without the coupling when the eccentric distance is 9 mm and the eccentric angle is 0°. This situation can easily lead to misdetection, and the variation patterns under other eccentric distances are similar to this.

3.4. The influence of coupling defects on the variation of magnetic flux density

Due to the complexity of the formation structure and the corrosive effects of liquids such as crude oil, the pipe couplings may experience varying degrees of damage. The following section separately studies the impact of the depth and size of coupling defects on the detection.

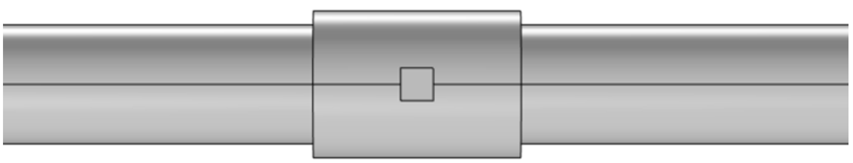

Fig.4 Schematic diagram of coupling defects.

The depth of the coupling defect is set as the only variable, with other variables kept constant. The defect radius is set to 10 mm, and the defect depths are tested at 2 mm, 4 mm, 6 mm, and 8 mm. The axial component of the magnetic flux density at the detection points is obtained through a parametric scan, as shown in Fig 5. Then, the radius of the coupling defect is set as the only variable, with other variables kept constant. The depth of the defect is 8 mm, and the defect radii are tested at 5 mm, 10 mm, 15 mm, and 20 mm. The axial component of the magnetic flux density at the detection points is obtained through a parametric scan, as shown in Fig 6.

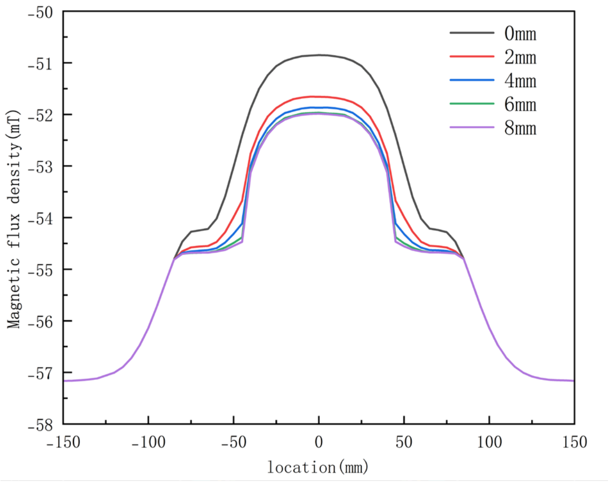

Fig.5 Variation of axial magnetic flux density with defects of different depths

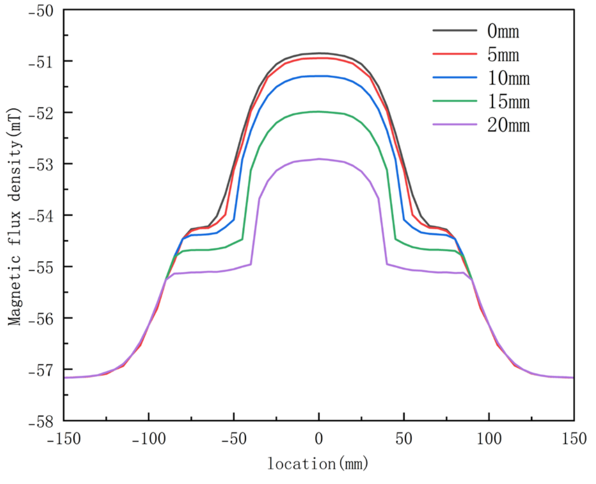

Fig.6 Magnetic flux density corresponding to defects of different radii.

Through simulation, the changes in magnetic flux density when the coupling has defects lead to the following conclusions: When the coupling has defects, the magnetic flux density differs significantly from when there are no defects. As the defect depth increases, the axial magnetic flux density extremum decreases. Similarly, as the defect radius increases, the axial magnetic flux density extremum also decreases. Additionally, with changes in the defect radius, the extremum part of the signal pattern becomes narrower, and the variation in magnetic flux density also decreases.

4. Coupling detection experiment

To verify the accuracy of the simulation analysis, an experimental platform for pipe coupling defect detection was built, as shown in Fig 7. It mainly consists of the experimental stand, the pipe coupling detection device, the pipe under test, and the host computer. The role of the experimental stand is to ensure that the pipe is centered during the detection process. The pipe coupling detection device includes a magnetization module and a detection module. The magnetization module provides a constant magnetic field through neodymium iron boron permanent magnets. The detection module consists of Infineon TLV493-A1B6 3D sensors and an Arduino Uno development board. The sensors are evenly arranged in the middle of the detection device and are connected to the host computer via a USB interface to collect axial, radial, and circumferential magnetic flux density signals. The pipe under test is connected to the coupling via threads, with a total length of 1000 mm. The role of the host computer is to display and store the signals collected by the pipe coupling detection device.

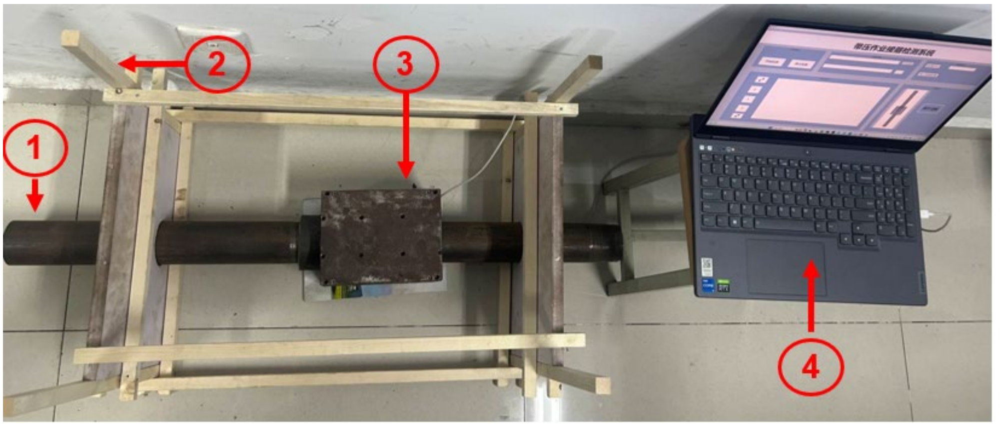

1-Measured pipe 2-Test rack 3-Pipe coupling detection device 4-Upper computer

Fig.7 Experimental platform diagram.

4.1. Signal collection and analysis

During the experiment, the pipe was moved at a constant speed for detection. The detection speed was divided into two types: fast and slow. For each type of experiment, a set of pipe coupling detection data was collected. To facilitate signal observation, the fast group used 800 sampling points for analysis, while the slow group used 1000 sampling points for analysis. As shown in Fig 8, it can be observed that the experimental signal undergoes significant changes when the coupling passes. The magnetic flux density when the pipe passes is about 21.75 mT, and the magnetic flux density when the coupling passes is about 15.11 mT, with a magnetic flux change of 6.64 mT. This proves that the pipe coupling detection method based on magnetic field sensing is effective and feasible.

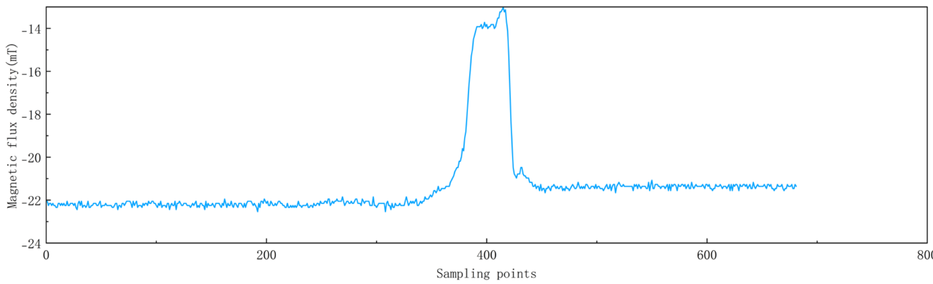

(a) fast group

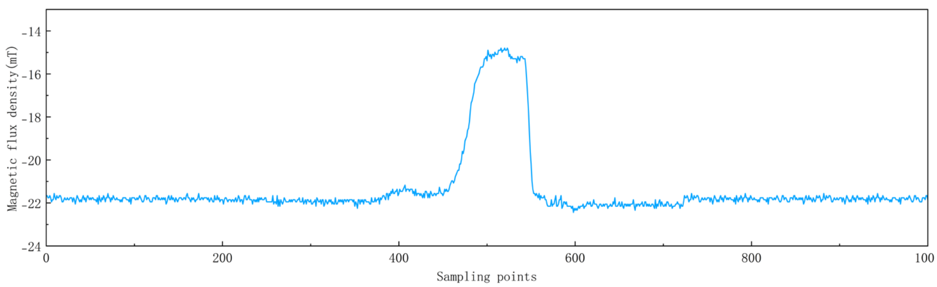

(b) slow group

Fig. 8 Pipe coupling detection experimental results diagram.

5. Conclusion

This study investigates the application of the magnetic field sensing method in pipe coupling detection. Through finite element simulation, the influence of various factors on the detection performance is analyzed. When the pipe and coupling pass through the detection device, they affect the uniformly distributed magnetic field within the device. The axial component of the magnetic flux density decreases when the coupling passes. The study also simulates and analyzes the influencing factors in pipe coupling detection, including the spacing between magnetic materials, magnetization intensity, pipe eccentricity, and coupling defects. The change in magnetic flux density decreases as the spacing between magnetic materials increases. The stronger the magnetization intensity, the greater the change when the pipe and coupling pass through the detection device. Pipe eccentricity has a significant impact on detection. Coupling defects also affect the detection, as defects alter the extreme values of the signal. Finally, experiments confirm that the pipe coupling detection method based on magnetic flux sensing is feasible.

References

[1] Dost, Y.,Apaydın,et al.(2012).Non-destructive testing of Bosphorus Bridges. RILEM Bookseries,6: 819-825. doi: 10.1007/978-94-007-0723-8_117

[2] F.I. Al-Naemi,J.P. Hall,A.J. Moses.(2006). FEM modelling techniques of magnetic flux leak-age-type NDT for ferromagnetic plate inspections. Journal of Magnetism and Magnetic Mate-rials,304(2): e790-e793. doi: 10.1016/j.jmmm.2006.02.225

[3] Jomdecha, C.,Prateepasen,et al.(2009). Design of modified electromagnetic main-flux for

steel wire rope inspection.[J]. NDT and E International,42(1): 77-83. doi: 10.1016/j.ndteint.2007.10.006

[4] Ni, XH ,et al.(2014). Research and Application Survey of Coupling Alarm in Pressure Opera-tion. INTERNATIONAL CONFERENCE MACHINERY, ELECTRONICS AND CONTROL SIMULATION,614: 672-675. doi: 10.4028/www.scientific.net/AMM.614.672

[5] Qun LEI,Dingwei WENG,Jianhui LUO. (2019). Achievements and future work of oil and gas production engineering of CNPC. Petroleum Exploration and Development,46(1): 145-152. doi: 10.1016/S1876-3804(19)30014-X

[6] Qun LEI, Yiliang LI, Tao LI, Hui LI, Baoshan GUAN, Guoqiang BI, et al.(2020). Technical status and development direction of workover operation of PetroChina. Petroleum Exploration and Development,47: 161-170. doi:10.11698/PED.2020.01.15

[7] Sorabh,Gupta, A.,et al.(2016). Finite Element Modeling of Magnetic Flux Leakage from Metal Loss Defects in Steel Pipeline(Article). Journal of Failure Analysis and Prevention,16(2): 316-323. doi: 10.1007/s11668-016-0073-6

[8] Shi, MJ,et al. (2018). Study on detection methods of residual wall thickness for process pipe-line corrosion in oil and gas gathering and transportation station(Article). Journal of Magnet-ics,23(2): 142-151. doi: 10.4283/JMAG.2018.23.2.142

[9] Wang, YK ,et al.(2019). Research on intelligent alarm method of coupling about snubbing operation in oil and gas field(Conference Paper). IOP Conference Series: Earth and Environ-mental Science,252(5): 052114. doi: 10.1088/1755-1315/252/5/052114

[10] Zhong, GX,et al.(2011). The Structure and Technical Parameters Analysis of Snubbing Unit. ADVANCED MANUFACTURING SYSTEMS,339: 566-570. doi: 10.4028/www.scientific.net/AMR.339.566